Rational Design of Supported PdAu Nanoparticle Catalysts from Structured Nanoparticle Precursors

ARTICLE *in* THE JOURNAL OF PHYSICAL CHEMISTRY C · JULY 2009

Impact Factor: 4.77 · DOI: 10.1021/jp9037182

Rational Design of Supported PdAu Nanoparticle Catalysts from Structured Nanoparticle Precursors

Priyabrat Dash,[†] Toby Bond,[†] Candace Fowler,[†] Wenbo Hou,[†] Neil Coombs,[‡] and Robert W. J. Scott*,[†]

Department of Chemistry, University of Saskatchewan, 110 Science Place, Saskatoon, Saskatchewan, Canada, and Department of Chemistry, University of Toronto, Toronto, Ontario, Canada

Received: April 22, 2009; Revised Manuscript Received: May 21, 2009

A series of poly(vinylpyrrolidone) (PVP)-stabilized metallic and bimetallic PdAu nanoparticles (coreduced and core−shell) with narrow size distributions were encapsulated into alumina matrixes by sol−gel chemistry, and their chemical, structural, electronic, and catalytic behaviors were investigated. Monodisperse nanoparticles were uniformly distributed in the alumina frameworks as observed by TEM images, and single-particle energy-dispersive spectroscopy (EDS) analyses confirmed the high compositional uniformity of the bimetallic nanoparticles. A combination of TEM, EDS mapping, TGA, XANES and EXAFS studies were used to fully characterize the alumina-supported nanoparticles before and after thermal treatments. It was observed that the size distribution of the final PdAu nanoparticles was highly dependent on calcination conditions, and careful high-temperature calcinations at 300 °C could be used to remove organic PVP stabilizers with minimal particle aggregation and/or structural transformations. The resulting supported nanoparticle catalysts were found to be active as hydrogenation catalysts. EXAFS analysis of coreduced PdAu nanoparticles indicated they had near-alloy structures with slightly Au-rich cores and Pd-rich shells before and after calcination, while intentionally designed Pd-core Au-shell nanoparticles retained their structures after calcination. XANES spectra of both coreduced and core−shell PdAu nanoparticles were also examined and showed that the PdAu coreduced nanoparticles had fewer Au valence d-band vacancies in comparison to monometallic nanoparticles while the PdAu core−shell nanoparticles had relatively higher Au valence d-band vacancies than the coreduced PdAu nanoparticles.

1. Introduction

Supported metal nanoparticle catalysts have long been used as heterogeneous catalysts in a number of industrially important catalytic reactions such as hydrogenations, dehydrogenations, hydrocracking, and reduction and oxidation reactions in fuel cells.[1,2] For many systems, bimetallic catalysts have been shown to have synergetic catalytic performances which differ from either of their individual metal components.[3−5] Palladium−gold is a bimetallic system which has been widely explored; for example, Hutchings et al. have shown that PdAu catalysts have a 25-fold increase in activity for the oxidation of alcohols to aldehydes as compared to pure Au or Pd catalysts.[6] Bimetallic PdAu nanoparticles have also shown excellent catalytic performance for the direct synthesis of H_2O_2 from H_2 and O_2,[7−13] glycerol oxidation,[14,15] the hydrochlorination of acetylene,[16] and many other reactions.[17−25] For many applications, it is desirable to fabricate heterogeneous supported nanoparticle catalysts for applications. Traditional synthetic techniques of supported nanoparticle catalysts for industrial applications typically involve the deposition of metal precursors onto high surface area supports, followed by various thermal activation treatments (incipient wetness method or deposition−precipitation).[26] The size distribution of nanoparticles and the degree of dispersion on the support are each highly dependent on the pH and concentration of the precursor solution, type of the oxide support, and calcination temperature and procedure.[26,27] In addition, these methods often provide limited control over the composition and structures of bimetallic nanoparticles, which often leads to significant compositional nonuniformity from particle to particle.[28] Poor control over compositional homogeneity and size of bimetallic nanoparticles often provides a serious challenge in understanding the size−structure−property relationships of bimetallic and multimetallic catalysts.

In order to address these issues, we fabricated supported PdAu nanoparticle catalysts by controlling the size, structure, and composition of coreduced and sequentially grown PdAu nanoparticles via well-established solution synthetic routes using poly(vinylpyrrolidone) (PVP) stabilizers. This was followed by incorporating the presynthesized nanoparticles into sol−gel syntheses of alumina. This route provides an alternative method of designing industrially relevant, supported nanoparticle catalysts through a rational chemical approach, leading to well-dispersed PdAu nanoparticles within high surface area alumina supports and good control over the size, composition, and internal structure of the nanoparticles. However, one of the pitfalls of this route as described above is that the PVP stabilizers must be removed without destroying the size and compositional and structural integrity of the prefabricated nanoparticles in order to produce the desired supported nanoparticle catalysts. Careful low-temperature calcination temperatures were employed to remove the PVP polymer. A combination of HRTEM, energy dispersive spectroscopy (EDS) mapping, thermal gravimetric analysis (TGA), and X-ray absorption near-edge and fine structure spectroscopy (XANES and EXAFS) studies were

* To whom correspondence should be addressed. E-mail: robert.scott@usask.ca. Telephone: 306-966-2017. Fax: 306-966-4730.
[†] University of Saskatchewan.
[‡] University of Toronto.

10.1021/jp9037182 CCC: $40.75
Published on Web 06/15/2009

carried out to allow for detailed characterization of the PdAu nanoparticle precursors before and after removal of the polymer stabilizers via low-temperature calcinations. Finally, the activity of the catalysts was evaluated using the well-studied hydrogenation reaction of a model substrate, allyl alcohol.

Among the various techniques available for the synthesis of supported bimetallic nanoparticle catalysts, the method of entrapping presynthesized nanoparticles into an inorganic matrix by the sol−gel method is an interesting route which has been investigated by other groups in the past.[29−31] This route takes advantage of the large number of synthetic solution protocols that have been developed to carefully control metallic and bimetallic nanoparticle sizes, shapes, and compositions.[20] Poly(*N*-vinyl-2-pyrrolidone) (PVP) is one of the most commonly used polymers for nanoparticle stabilization and catalysis, as it allows synthesis of stabilized nanoparticles with accessible surface areas in polar solvents such as water.[5,32,33] After successful synthesis and purification, the nanoparticle precursors, in which the particle size distribution, composition, and structure is well-defined, are then deposited onto various supports to synthesize highly dispersed heterogeneous bimetallic catalysts.[34,35] In recent years, nanoparticles synthesized by dendrimers,[17,36−41] monolayers,[42−46] and polymer stabilizers[5,47,48] have been used as precursors for supported nanoparticle catalysts. Entrapping presynthesized metal nanoparticles, including PdAu nanoparticles, into an inorganic matrix by sol−gel chemistry is an attractive route that has been used by several groups.[17,30,36,43,47,49] For example, Parvulescu and co-workers synthesized heterogeneous PdAu catalysts by embedding preprepared tetraalkylammonium-stabilized PdAu nanoparticles in a sol−gel SiO_2 matrix.[49] More recently, Crooks and co-workers synthesized PdAu/TiO_2 catalysts using dendrimer-stabilized nanoparticles by a sol−gel route.[17] In both cases this approach produced a narrow distribution of PdAu nanoparticles in the oxide support after the stabilizer was removed by calcination. However, in neither of these cases was the structural integrity of the nanoparticle followed before and after calcination.

An area of concern in designing supported nanoparticle catalysts from presynthesized nanoparticles is nanoparticle sintering, alloying/segregation, and metal oxidation upon removal of the organic stabilizers via thermal treatments.[42,50] Sintering of the metal is strongly temperature-dependent, and thus, coalescence of metal particles often occurs at the Tammann temperature, which is half of the melting point.[51] For example, gold nanoparticles supported on silica support tend to form very large agglomerates above Tammann temperatures of Au.[52] This is a rather complicated problem in the PdAu bimetallic system due to the segregation tendency of these metals.[19,53,54] For example, Hutchings and co-workers found that degree of segregation increases with temperature in the PdAu/Al_2O_3 system.[19] After calcination, the particles began to exhibit surface enrichment of Pd, and sintering of the Pd particles on the support surface had occurred. Thus, removal of the organic stabilizer(s) in order to activate supported nanoparticle catalysts is not a trivial problem, and much care must be taken such that size, composition, and structure are retained after thermal treatments.

Though HRTEM and EDS mapping techniques can help follow the average particle size and compositions before and after thermal treatment, in general they do not give much information as to surface vs bulk atomic distributions. X-ray absorption spectroscopy comprising both X-ray absorption near-edge spectroscopy (XANES) and extended X-ray absorption fine structure spectroscopy (EXAFS) has been a used as valuable tool for the examination of PdAu and other bimetallic nanoparticle structures by the catalyst community in the past.[4,32,55−60] While XANES can reveal the oxidation state and d-occupancy of a specific atom type,[61,62] EXAFS provides a valuable tool for the analysis of local atomic structure, giving information about the average local atomic coordination environment.[63,64] When combined with adequate models of the nanoparticle structure and composition, EXAFS measurements of carefully synthesized nanoparticles can be used to shed light on possible structures of such nanoparticles. Thus EXAFS has the ability to give quantitative information of the nanoparticle structure before and after thermal treatments of nanoparticles, which can be critical in designing any industrially relevant heterogeneous catalysts.[65,66]

Herein, we report a rational chemical method for the synthesis of heterogeneous catalysts based on coreduced and sequentially grown PdAu nanoparticles trapped in alumina matrixes. Low-temperature calcination conditions (∼300 °C) were found to be optimal for the removal of the PVP polymer stabilizer with minimal changes in the average particle size, composition, and structure. The structural, chemical, and electronic properties of the supported nanoparticle catalysts were characterized by transmission electron microscopy and EDS mapping, thermal analysis (TGA), and X-ray absorption spectroscopy (EXAFS, XANES). EXAFS analysis of coreduced PdAu nanoparticles indicated they had near-alloy structures with slightly Au-rich cores and Pd-rich shells before and after calcination, while intentionally designed Pd-core Au-shell nanoparticles retained their structures after calcination. The XANES spectra of coreduced PdAu nanoparticles showed that the PdAu coreduced nanoparticles had fewer Au valence d-band vacancies in comparison with monometallic nanoparticles while the PdAu core−shell nanoparticles had relatively higher Au valence d-band vacancies compared to the coreduced PdAu nanoparticles. Extensive characterization of these supported PdAu catalysts shows that a rational design methodology is effective for the synthesis of heterogeneous catalysts in which the structural and compositional integrity of predesigned nanoparticles is maintained in the final heterogeneous supported nanoparticle catalysts.

2. Experimental Methods

2.1. Materials. Poly(vinylpyrrolidone) (MW 40 000), hydrogen tetrachloroaurate hydrate (99.9%), potassium tetrachloropalladate (99.99%), aluminum isopropoxide (98%), and allyl alcohol (99%) were purchased from Alfa and were used without further purification. Ascorbic acid (99.7%), isopropyl alcohol (99.8%), and nitric acid (38−40%) were purchased from EMD and were used as obtained. Sodium borohydride powder (98%) was obtained from Aldrich and was used as obtained. Deuterated solvents were purchased from Cambridge Isotope Laboratories. Eighteen MΩ·cm Milli-Q water (Millipore, Bedford, MA) was used throughout. Cellulose dialysis membranes (MW cutoff 12 400 g/mol) were purchased from Aldrich.

2.2. Synthetic Methods. ***Nanoparticle Synthesis.*** The procedure for synthesizing PVP-stabilized Au, Pd, and coreduced PdAu nanoparticles in methanol was described previously.[24,67] Methanol was removed from the nanoparticle solution under vacuum, followed by the addition of the same volume of isopropanol to synthesize the nanoparticles in isopropanol. The procedure for synthesizing PVP-stabilized sequentially grown 1:3 Pd:Au core−shell nanoparticles from Pd nanoparticle seeds is as follows:[38] PVP-stabilized Pd nanoparticle seeds were prepared by adding 10.0 mL of a 10 mM K_2PdCl_4 solution and 20.0 mL of 1.39 mM PVP in 4.4 mL of water followed by

stirring under nitrogen for 30 min. Two milliliters of 0.10 M $NaBH_4$ solution was then added, followed by stirring for 30 min. The solution was then dialyzed overnight under nitrogen. After dialysis, 3.15 mL of the Pd seed solution was added to a round-bottomed flask followed by addition of 79.5 μmol of ascorbic acid under N_2. In a separate vial, 265 μL of a 0.10 M ascorbic acid solution was added to 2.65 mL of 0.010 M $HAuCl_4$ and 13.2 mL of deionized water, giving a colorless solution. Core−shell 1:3 Pd:Au nanoparticles (1.75 mM) were then synthesized by rapidly adding the "Au^{+}"/ascorbic acid solution to the Pd seed solution followed by stirring for 30 min.[68] The alumina-supported 1:3 Pd:Au core−shell nanoparticle catalysts were then prepared according to the methods described below.

Sol−Gel Chemistry. All sol−gel chemistry was carried out under nitrogen. PVP-stabilized Au, Pd, and bimetallic PdAu nanoparticles in isopropanol were used to prepare Al_2O_3-supported catalysts with 2.5 wt % metal loading. Dilute aqueous nitric acid (2 mL, 5 wt %) was added dropwise to the nanoparticle solution, followed by the addition of 0.51 g of $Al(O^iPr)_3$ dissolved in 5.0 mL of freshly dried isopropanol. Within 50−60 s, a gel was formed and was left overnight to age. The filtrate was then removed from the gel by simple decantation. In all cases the filtrate was completely colorless, confirming the trapping of all the nanoparticles in the alumina matrix. The powder was then dried in an oven at 150 °C for 3 h to give the as-synthesized xerogel-supported nanoparticles. The as-synthesized samples were then calcined in a furnace at 300 °C for 5 h in flowing air followed by reduction under H_2 flow at 300 °C for 1 h to remove the PVP stabilizer. The same procedure above was followed for the synthesis of Pd, Au, 3:1, 1:1, 1:3 $PdAu/TiO_2-Al_2O_3$ catalysts, keeping the total metal concentration constant.

2.3. Characterization. Thermogravimetric analysis (TGA) was performed using a TA Instruments TGA Q5000IR under air flow. Initial samples were run from 25 to 600 °C with a heating rate of 10 °C/min to determine the total amount of PVP polymer present and the degradation temperature range. This was followed by running separate samples which were held for 5 h at the onset of PVP degradation temperature while monitoring the total mass loss of the sample. TEM micrographs were obtained with a Philips 410 microscope operating at 100 keV, while HRTEM investigations were performed using a Hitachi HD-2000 microscope with a field emission cathode at 200 kV. STEM images were recorded with a high-angle annular dark-field (HAADF) detector. The sample was prepared by placing a drop of the methanol solution of a well-ground catalyst powder onto a carbon-coated copper grid (200 Mesh, Electron Microscopy Sciences) followed by evaporation of the methanol. EDS line scan data were collected using an acceleration voltage of 200 kV, a collection time of 60 s, and a 0.5 nm diameter probe. Integrated intensities obtained from the Pd $L_{\alpha 1}$ and Au $L_{\alpha 1}$ lines were used for quantification of the two metals, respectively, because they did not overlap the other X-ray emission lines. XRD measurements were carried out using a Rigaku Rotaflex RU-200 diffractometer using the Cu K_α radiation line; the sample was scanned over the 2θ range of 5−80°.

X-ray absorption spectra at the Pd K-edge and the Au L_{III}-edge were recorded at the HXMA beamline 061D-1 (energy range, 5−30 keV; resolution, 1×10^{-4} $\Delta E/E$) at the Canadian Light Source (CLS, 2.9 GeV storage ring, 250 mA current). All samples were pressed into pellets and measured in transmission mode at room temperature. A double-crystal Si(111) monochromator was employed for energy selection at both Au L_{III}-edge (11 919 eV) and Pd K-edge (24 350 keV). Higher harmonics were eliminated by detuning double-crystal Si(111) by using a Rh-coated 100 mm long KB mirror. The incident and transmission X-ray intensities were detected by ion chambers filled with helium−nitrogen mixtures that were installed in front of and behind the sample cell, while a third ionization chamber was present after the reference foil such that energy calibration could be performed for each scan. Energy was scanned from 200 eV below the edge to 1000 eV above the edge. Standard reference compounds, Pd foil and Au foil for the respective edges, were measured simultaneously.

Data processing was performed with the use of the software package IFEFFIT.[69] First, the raw absorption spectrum in the pre-edge region was fitted to a straight line, and the background above the edge was fit using a cubic spline function. The EXAFS function, χ, was obtained by subtracting the postedge background from the overall absorption and then normalizing with respect to the edge jump step. The normalized $\chi(E)$ was then Fourier-transformed from energy space to k-space. The $\chi(k)$ data were k^3-weighted in order to compensate for the dampening of the EXAFS amplitude with increasing k. k^3-weighted data were Fourier-transformed to r-space to separate the EXAFS contributions from different coordination shells. The EXAFS fitting was performed in r-space between 1.5–3.3 Å for Au-edge and 1.3−3.2 Å for the Pd-edge (without phase correction) using theoretical phase-shift and amplitude generated by FEFF 6.0 code.[70] A homogeneous PdAu alloy model for the FEFF fitting was constructed based on bulk PdAu lattice parameters reported in the literature.[71] The amplitude reduction factor, So^2, for Au and Pd was obtained by analyzing Au and Pd reference materials, respectively, and by fixing coordination numbers for the bulk fcc metals to be 12 in the FEFFIT input file.[72] The So^2 values were found to be 0.83 and 0.84 for Pd and Au, respectively.

2.4. Catalytic Test Reaction. The hydrogenation of allyl alcohol was performed in a three-necked round-bottomed flask at 40 °C. Initially, air trapped in the aqueous suspension of the catalysts (50 mg of catalyst in 10 mL of aqueous solution) was removed under vacuum. The procedure for the hydrogenation reaction was followed as described previously.[24] A H_2 gas source was connected to one end of the flask, while the other end with the differential pressure gauge (Model 407910, Extech Instruments Corp. with a resolution of 0.001 atm and accuracy of ±2% at 23 ± 5 °C) and the central portion was closed with a rubber septum. Initially, 10 mL of the nanoparticle catalyst aqueous solution was placed in the flask, followed by purging the system with H_2 for 10 min. Next, 0.50 mL of the allyl alcohol substrate was added under vigorous stirring conditions, followed by measurement of the H_2 uptake via differential pressure measurements every 10 s. The amount of hydrogen consumed was determined from the pressure decrease assuming hydrogen behaves as an ideal gas.[73] Correlation of hydrogen consumption and product formation (1-propanol) was found to be 100% (with an error of *ca.* 2%) via ^1H NMR experiments. This allowed the turnover frequency (TOF, (mol of product/mol of metal) h^{-1}) to be determined from the slope of linear plots of TON (mol of product/mol of metal) versus time.

3. Results and Discussion

Coreduced PdAu nanoparticles and sequentially grown 1:3 Pd:Au core−shell nanoparticles were synthesized according to literature protocols.[24,67] The coreduced PdAu nanoparticles (Pd:Au ratios of 3:1, 1:1, and 1:3) and pure Au and Pd nanoparticles all had average particle sizes ranging from 3.0 to 4.0 nm, and

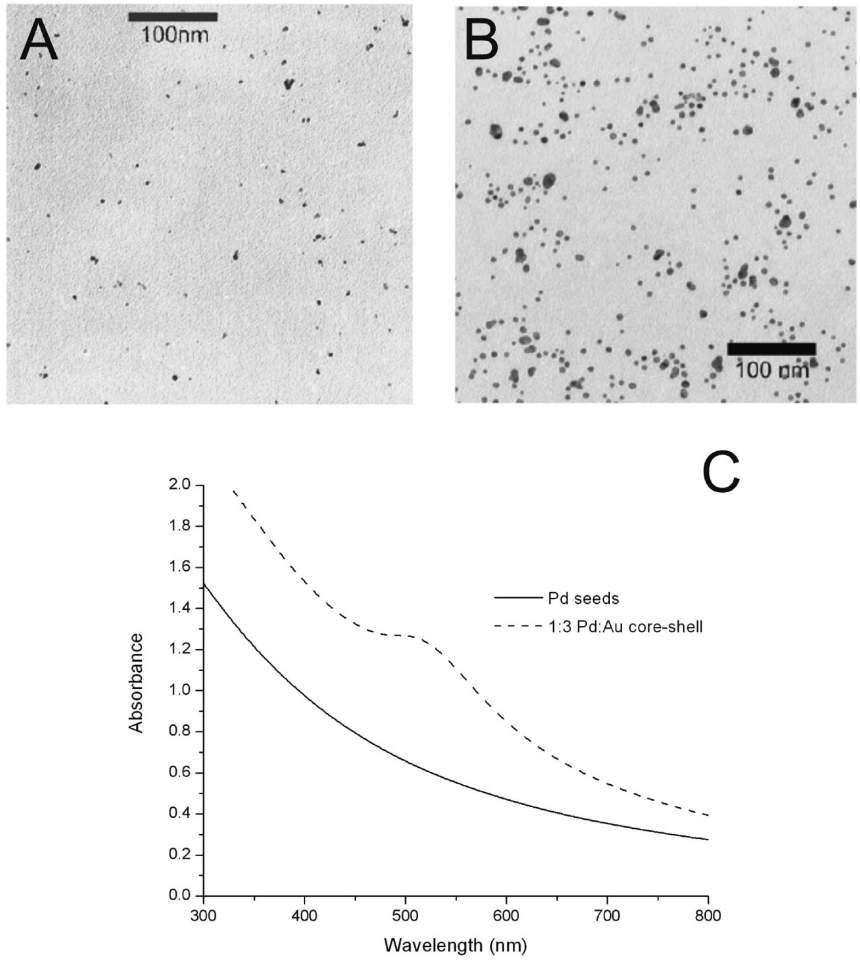

Figure 1. TEM images of PVP-stabilized (A) Pd seeds and (B) 1:3 Pd core-Au shell nanoparticles and (C) UV−vis spectra of Pd seeds and 1:3 Pd core−Au shell nanoparticles.

UV−vis spectra of the PdAu samples showed no separate Au plasmon peak at ~520 nm, confirming the formation of bimetallic random/alloy nanoparticles.[38,74] Pd−Au core−shell nanoparticles were synthesized by growing a successive gold shell on presynthesized Pd nanoparticle seeds.[38] Galvanic reactions of Au^{3+} salts with the Pd^0 nanoparticles were avoided by prereducing the $AuCl_4^-$ salt with ascorbic acid to form Au^+ salts prior to addition of the Au salts to the Pd nanoparticle seeds.[75] Figure 1 shows TEM images of the Pd seeds and sequentially grown 1:3 Pd:Au core−shell nanoparticles; the initial Pd seeds had an average particle size of 3.1 ± 1.7 nm, while after Au shell formation, the resulting 1:3 Pd:Au core−shell nanoparticles had an average size of 5.2 ± 1.8 nm. This size increase is consistent with the respective metal loadings of the core and shell, respectively, using eq 1[76]

$$D = D_{\text{core}}\left(1 + \frac{V_{\text{Au}}[\text{Au}]}{V_{\text{Pd}}[\text{Pd}]}\right)^{1/3} \quad (1)$$

where D_{core} is the diameter of the experimentally measured Pd core (3.1 nm) and V_{Au} and V_{Pd} and [Au] and [Pd] are the molar volumes and concentrations of Au and Pd, respectively. The molar volumes of gold and palladium used, V_{Au} and V_{Pd}, were 10.21 and 8.56 cm^3/mol, respectively. Using the average measured Pd nanoparticle size of 3.1 nm, eq 1 yields a diameter of 5.15 nm, which is fairly close to the value of 5.2 nm obtained from TEM measurements. UV−vis spectra of the Pd seeds and 1:3 Pd core−Au shell nanoparticles are shown in Figure 1C. Upon growth of a gold shell on the Pd seeds, a weak plasmon band around 520 nm develops. The presence of a Au plasmon band is consistent with ~2 nm Au shell growth over a Pd core; however, more conclusive evidence of core−shell formation via EDS line scans and EXAFS results for these nanoparticles trapped in alumina will be presented later.

After the bimetallic PdAu nanoparticles were synthesized, the particles were trapped in an alumina matrix through sol−gel chemistry. This involved the hydrolysis and condensation of a $Al(O^iPr)_3$ precursor in the presence of the PVP-stabilized nanoparticles, to give 2.5% by weight metal nanoparticles in an alumina support.[36] After gelation of the alkoxide precursor, expulsion of clear isopropanol occurred overnight, likely due to aging of the alumina gel (syneresis), indicating complete trapping of the PVP-stabilized particles in the gel. The mean particle sizes and size distributions of the as-synthesized nanoparticles dispersed in alumina matrixes were obtained by HRTEM images. For STEM studies, coreduced 1:1 PdAu nanoparticles were primarily studied as representative samples as they should contain approximately equal amounts of both metals, and thus should facilitate EDS studies. Figure 2A shows a dark-field HRTEM image of coreduced 1:1 PdAu nanoparticles dispersed in an amorphous alumina matrix. The particles are well dispersed within the oxide support, with an average nanoparticle size of 4.1 ± 0.7 nm. This is slightly larger than the average particle size of the original synthesized particles but is within error of the TEM technique.[77] Single-particle

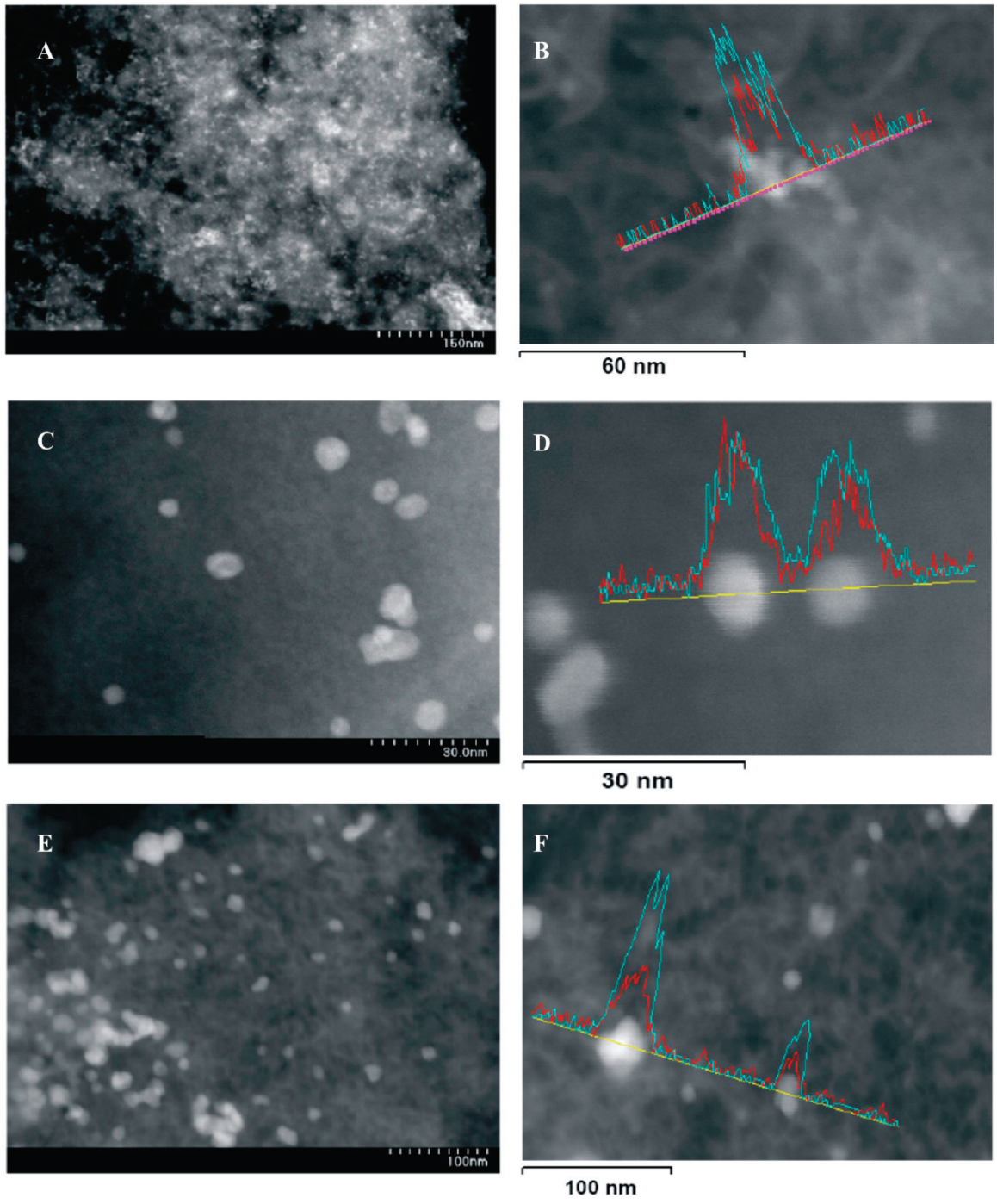

Figure 2. HRTEM images and EDS line scans of coreduced PVP-stabilized 1:1 Pd:Au nanoparticles (A) as-synthesized in alumina and (B) the corresponding EDS line scan; (C) in alumina calcined at 300 °C and (D) the corresponding EDS line scan; (E) in alumina calcined at 500 °C and (F) the corresponding EDS line scan. The blue and red EDS lines are Au and Pd, respectively.

energy-dispersive spectroscopy (EDS) analyses indicate an average composition of approximately 1:1 of Pd and Au (with a standard deviation of 10%), which is in agreement with the molar percentage of respective salts during the synthesis. Figure 2B shows an EDS line scan which unambiguously shows the presence of both salts in individual nanoparticles. This confirms the high compositional uniformity of the bimetallic nanoparticles.

Removal of the polymer stabilizer while maintaining the nanoparticle dispersion, composition, and size represents a great challenge in utilizing presynthesized nanoparticles to form heterogeneous catalysts. Industrial catalysts are typically activated by thermal methods in air or inert atmospheres followed by reduction to produce a clean, reduced catalyst. We wished to identify the lowest temperature conditions which could lead to complete removal of the PVP polymer while maintaining the integrity of the nanoparticles. The as-synthesized xerogel-supported nanoparticle samples were characterized by TGA to find out the total PVP wt % and the optimal calcination temperatures. As shown in Figure 3a, the TGA curve of the as-synthesized PdAu−alumina sample at a heating rate of 10 °C/min has two distinct weight losses, with water desorbed below 100 °C (∼10% mass loss) and PVP decomposition at 300−500 °C (∼41% mass loss). Based on these observations, samples were calcined at 500 °C under air for 5 h and then reduced under hydrogen at 300 °C for 1 h. As can be seen from Figure 2E, the particle sizes increased dramatically to 11.7 ±

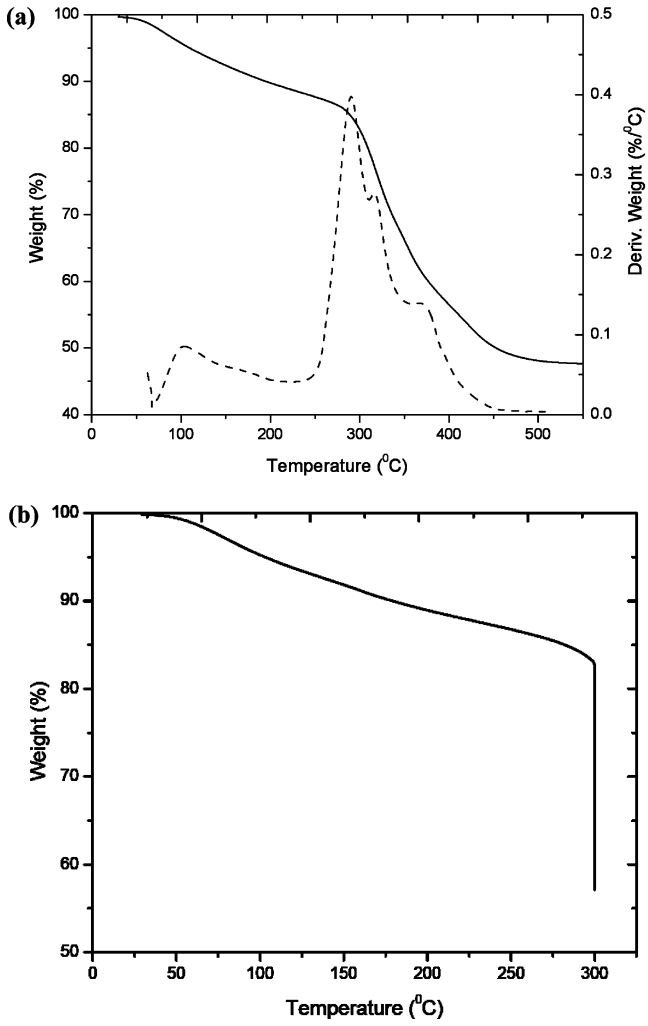

Figure 3. Thermal gravimetric analysis plots showing (a) mass loss and derivative of mass loss of PVP-stabilized 1:1 PdAu nanoparticles in alumina from 25 to 550 °C and (b) mass loss for the same sample held at 300 °C for 5 h.

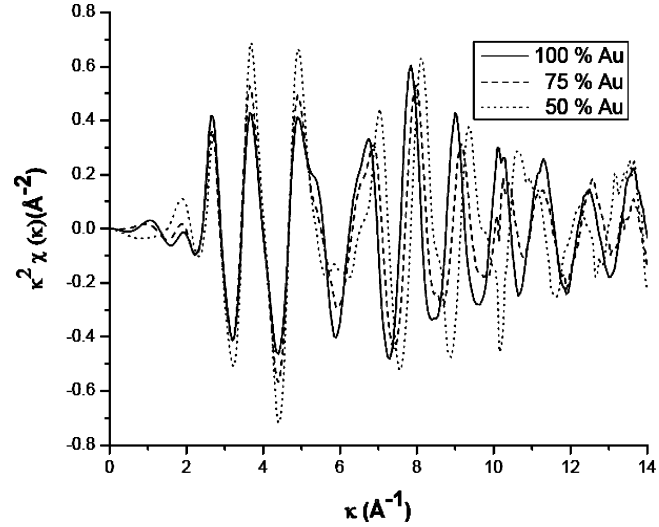

Figure 4. Au L_{III}-edge EXAFS in *k*-space for the coreduced nanoparticle series.

2.9 nm for coreduced 1:1 Pd:Au nanoparticles upon calcination at 500 °C, and a great deal of particle aggregation was seen. In addition, metal segregation was problematic, as seen in the EDS line scan in Figure 2F. To overcome these problems, we sought to find the minimal thermal activation calcination conditions needed by running TGA experiments at a temperature just above the onset of the polymer decomposition temperature (300 °C). As shown in Figure 3b, by holding the temperature at 300 °C for 5 h, a slightly lower mass % of polymer (~34% mass loss) was removed at lower calcination temperatures. After calcination at 300 °C for 5 h under air, followed by the reduction under hydrogen at 300 °C for 1 h, the average particle sizes for the supported- coreduced 1:1 Pd:Au nanoparticles increased from 4.1 ± 0.7 to 5.5 ± 1.4 nm (Figure 2C). This increase is much smaller than seen at higher temperatures, and it seems unavoidable to have some particle size increase due to sintering during calcination treatments. Single-particle EDS analyses of the coreduced 1:1 Pd:Au bimetallic nanoparticles calcined at 300 °C indicate the same average compositions (~1:1) as that of the as-synthesized sample; Figure 2D shows a EDS line scan across several particles. These results suggest that by properly choosing thermal treatment conditions it is possible, to some extent, to control the degree of sintering and hence the particle size and composition; however, some nanoparticle sintering seems unavoidable even with mild calcination conditions. In addition, the resulting particles calcined at 300 °C have been shown to be catalytically active, as will be discussed later. It should be noted that TEM and EDS measurements could not distinguish between surface and bulk compositions of the particles; EXAFS results detailed below will shed more light onto the bulk vs surface distributions of the elements within the nanoparticles. Powder XRD of the calcined alumina-supported catalysts revealed peaks at 38.0°, 45.6°, and 67.0° (2θ), which correspond to the γ-Al_2O_3 phase.[78]

To gain further insight into the interior architecture of coreduced PdAu nanoparticles trapped in alumina, XAS studies were carried out for both as-synthesized and calcined samples of coreduced PdAu nanoparticles, and pure Pd and Au nanoparticles at the Au L_{III}-edge and Pd K-edge. Initially, pure Au and Pd nanoparticles trapped in alumina were analyzed before and after calcination at 300 °C. Figure 4 shows representative EXAFS spectra at the Au L_{III}-edge of the coreduced nanoparticles before calcination; high-quality data was collected. It was found that the EXAFS oscillation frequencies and the features of the curves differ gradually from bulk gold to lower Au content in the bimetallic PdAu series, thus indicating some correlation between Pd and Au. This observation can be attributed to the formation of more Pd−Au bonds in the bimetallic samples.[79]

For the metallic and bimetallic nanoparticles, the Au and Pd EXAFS data of the same sample were simultaneously fit using the IFEFFIT software package.[72] Figure 5 shows the experimentally obtained Au and Pd EXAFS *r*-space for the coreduced PdAu nanoparticles and the single-shell theoretical fits; the structural parameters of the Pd:Au series generated from the EXAFS fitting parameters are presented in Table 1. As can be seen in Figure 5, good fits have been obtained for all samples, confirming the high-quality data of the samples. No attempt was made to fit weak shoulders at lower *r*-values in both the Au and Pd edges; these are likely due to contributions of the PVP polymer and the presence of trace levels of halide and oxide impurities bound on the surfaces.

For the as-synthesized monometallic Au and Pd nanoparticles, the nearest-neighbor coordination numbers (CNs), N_{Au-Au} and N_{Pd-Pd}, are 10.8 and 8.9, respectively, both smaller than 12 (Table 1). This implies the presence of smaller particles and, thus, relatively larger fractions of surface atoms, and that the Pd nanoparticles are significantly smaller than their Au counterparts.[79,80] For the gold nanoparticles, the interatomic

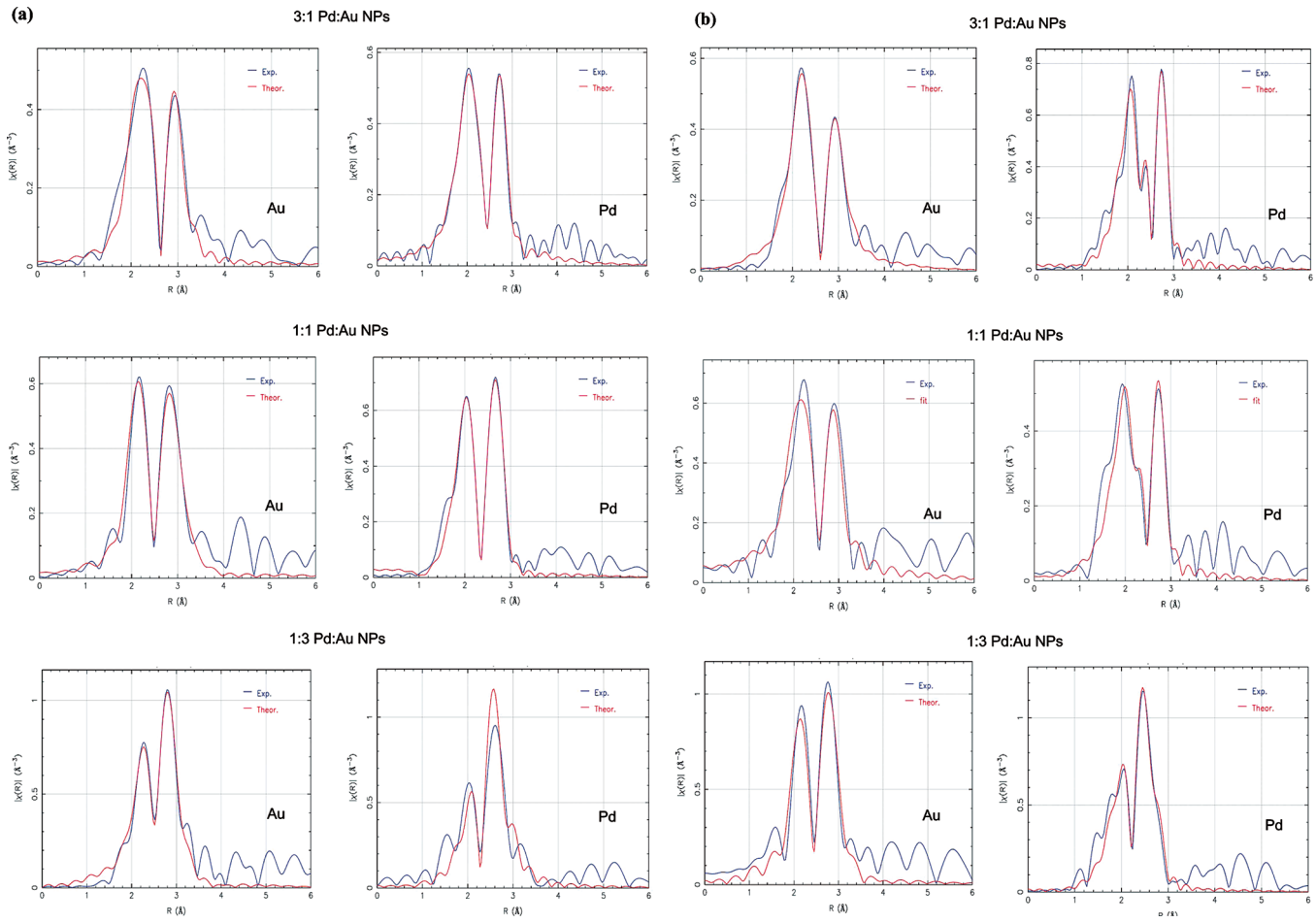

Figure 5. EXAFS single-shell fits for coreduced PdAu nanoparticle series (a) as-synthesized in alumina and (b) calcined at 300 °C.

TABLE 1: EXAFS Fitting Parameters of Pure Metals

sample	shell	N	R_j (Å)	ΔE_0 (eV)	σ^2 (Å^2)	R-factor
pure Au (as-synthesized)	Au−Au	10.8 (0.5)	2.838 (0.046)	4.2(0.3)	0.010 (0.001)	0.006
pure Au (calcined)	Au−Au	11.3 (0.5)	2.858 (0.026)	5.5(0.2)	0.008 (0.001)	0.005
pure Pd (as-synthesized)	Pd−Pd	8.9 (0.9)	2.732 (0.018)	−7.0(0.6)	0.006 (0.001)	0.016
pure Pd (calcined)	Pd−Pd	9.6 (1.1)	2.731 (0.019)	−5.8(0.7)	0.007 (0.001)	0.005
Au foil	Au−Au	12	2.861 (0.023)	5.2(0.3)	0.008 (0.001)	0.008
Pd foil	Pd−Pd	12	2.743 (0.007)	−5.3(0.5)	0.005 (0.001)	0.004

distance is 0.02 Å smaller than the bulk value of 2.86 Å. This decrease can be attributed to the increased d−d interaction in small particles due to hybridization.[65,81] Similarly, the Pd−Pd bond distance in Pd/Al_2O_3 is 2.73 Å, compared to the bulk distance of 2.74 Å.[82] After calcination of the pure Au and Pd samples at 300 °C, slight increases in CNs were observed (Table 1). The Au−Au CN (N_{Au-Au}) in the calcined Au/Al_2O_3 system increased from 10.8 to 11.3 after calcination, while in the case of the Pd/Al_2O_3 system, the N_{Pd-Pd} CN increased from 8.9 to 9.6 after calcination. This indicates that there is a moderate particle size increase due to sintering occurring in both samples.

In order to interpret the EXAFS parameters of the as-synthesized coreduced PdAu nanoparticles, the total CNs around each metal are calculated as follows: $N_{Au-M} = N_{Au-Au} + N_{Au-Pd}$ and $N_{Pd-M} = N_{Pd-Pd} + N_{Pd-Au}$. The total metal CNs, N_{Au-M} and N_{Pd-M}, for all three members of the PdAu series (before and after calcination) are smaller than that expected for bulk fcc alloys (i.e., 12). This is due to the large number of undercoordinated surface atoms on the surface of the particles.[79] Looking at the three as-synthesized coreduced PdAu samples in Table 2, it is noted that the N_{Pd-M} and N_{Au-M} CNs change linearly with Pd and Au concentration, which would be expected for ideal random alloys.[83] However, careful observation on the CNs indicated that N_{Au-M} CNs exceed N_{Pd-M} CNs for all of the as-synthesized bimetallic PdAu nanoparticle samples. In addition, the N_{Pd-Au} CNs for each of the samples are generally higher than anticipated compared to their N_{Au-Pd} values (for a true bulk alloy, N_{Au-Pd} should be equal to (mol Pd/mol Au) × N_{Pd-Au}). Both of these observations are consistent with the presence of slightly more Pd atoms on the surface of the particles than the bulk, and thus the particles are not true alloys but have slightly Au-rich cores and Pd-rich shells. In the case of 3:1 Pd:Au nanoparticles, the value of the N_{Au-M} CN is ∼12, which indicates that the Au atoms nearly all reside in the core of the nanoparticle. We are uncertain as to the reasons for this deviation from alloy behavior in the as-synthesized coreduced PdAu samples, but note that other groups have reported similar findings.[32,79,83,84] Several possible explanations include the presence of slightly faster kinetics for Au reduction vs Pd reduction upon synthesis of the nanoparticles with $NaBH_4$, surface segregation of the Pd to the surface due to oxidation, or preferential binding of the PVP stabilizer to Pd thus pulling Pd to the surface of the

TABLE 2: EXAFS Fitting Parameters of PdAu Nanoparticle Series

sample	shell	N	R_j (Å)	ΔE_0 (eV)	σ^2 (Å^2)	R-factor
1:3 Pd:Au (as-synthesized)	Au−Au	8.0 (1.5)	2.798 (0.008)	4.7(0.5)	0.010 (0.002)	0.016
	Au−Pd	1.9 (0.6)	2.770 (0.005)		0.010 (0.001)	
	Pd−Pd	0.7 (0.2)	2.749 (0.015)	−6.2(0.4)	0.006 (0.002)	
	Pd−Au	8.9 (0.6)	2.770 (0.005)		0.010 (0.001)	
1:3 Pd:Au (calcined)	Au−Au	9.2 (1.4)	2.808 (0.043)	4.6(0.5)	0.011 (0.002)	0.007
	Au−Pd	1.8 (0.4)	2.794 (0.056)		0.008 (0.001)	
	Pd−Pd	2.1 (1.1)	2.739 (0.112)	−6.1(0.7)	0.008 (0.004)	
	Pd−Au	8.8 (1.5)	2.794 (0.056)		0.008 (0.001)	
1:1 Pd:Au (as-synthesized)	Au−Au	7.0 (2.3)	2.801 (0.016)	4.7(0.6)	0.010 (0.004)	0.004
	Au−Pd	4.2 (0.8)	2.777 (0.040)		0.010 (0.001)	
	Pd−Pd	3.6 (0.3)	2.776 (0.040)	−5.8(0.2)	0.010 (0.001)	
	Pd−Au	7.2 (0.4)	2.777 (0.040)		0.010 (0.001)	
1:1 Pd:Au (calcined)	Au−Au	9.2 (2.5)	2.782 (0.035)	1.7(1.2)	0.008 (0.002)	0.016
	Au−Pd	2.7 (1.0)	2.770 (0.047)		0.009 (0.002)	
	Pd−Pd	3.0 (1.6)	2.726 (0.091)	−6.4(1.0)	0.012 (0.005)	
	Pd−Au	6.9 (1.8)	2.770 (0.047)		0.009 (0.002)	
3:1 Pd:Au (as-synthesized)	Au−Au	5.1 (2.6)	2.834 (0.030)	4.4(1.2)	0.009 (0.006)	0.019
	Au−Pd	7.1 (1.9)	2.866 (0.020)		0.009 (0.002)	
	Pd−Pd	7.2 (1.5)	2.779 (0.010)	1.9(0.8)	0.009 (0.002)	
	Pd−Au	2.6 (1.6)	2.866 (0.020)		0.009 (0.002)	
3:1 Pd:Au (calcined)	Au−Au	5.3 (3.1)	2.777 (0.026)	4.8(1.1)	0.006 (0.006)	0.018
	Au−Pd	6.1 (1.5)	2.772 (0.014)		0.007 (0.002)	
	Pd−Pd	6.4 (0.9)	2.746 (0.008)	−6.5(0.5)	0.007 (0.001)	
	Pd−Au	4.1 (1.1)	2.772 (0.014)		0.007 (0.002)	
core−shell	Au−Au	10.1 (0.8)	2.850 (0.002)	5.5(0.4)	0.008 (0.000)	0.013
1:3 Pd:Au (as-synthesized)	Au−Pd	0.9 (0.6)	2.798 (0.053)		0.008 (0.004)	
	Pd−Pd	8.1 (2.1)	2.772 (0.079)	−7.8(1.0)	0.008 (0.002)	
	Pd−Au	4.0 (2.4)	2.798 (0.053)		0.008 (0.004)	
core−shell	Au−Au	8.8 (2.4)	2.850 (0.004)	6.2(1.3)	0.006 (0.003)	0.013
1:3 Pd:Au (calcined)	Au−Pd	2.3 (1.3)	2.801 (0.044)		0.006 (0.004)	

nanoparticles. However, it should be noted that all as-synthesized samples were kept under nitrogen during synthesis and prior to EXAFS analysis. The coordination numbers obtained from EXAFS analysis can be a strong function of the particle size if the particle size is small (3−5 nm) and the particle size distribution is narrow.[82] This behavior has been used by others in EXAFS analysis to estimate average particle sizes.[64,66] The average of the first-shell N_{Au-M} and N_{Pd-M} CNs of the 1:1 Pd:Au system is found to be 11.0, indicating an average particle size from EXAFS of approximately 4.6 nm, which is close to the value of 4.1 nm obtained from HRTEM measurement.[66]

The calcined (300 °C) coreduced PdAu materials also show higher total Au CNs than Pd CNs ($N_{Au-M} > N_{Pd-M}$) as was observed in the particles prior to calcination, which indicates that structures were fairly well preserved after the thermal treatment method (Figure 5b, Table 2). Others have previously noted PdAu alloy to Au core−Pd shell transitions upon calcination and/or ligand extractions, presumably due to Pd metal oxidation and rereduction during the synthesis;[19,83] however, no increase in Pd surface segregation occurred for the calcined samples, likely due to the low calcination temperatures employed in this work. It should be noted that due to fairly high CN errors in EXAFS analysis (∼15−20%) it is extremely difficult to monitor small changes in Pd and Au bulk-vs-surface speciation by EXAFS. In the calcined samples, the Au−Au bond distance decreases with increasing Pd content, from 2.81 Å in the 1:3 Pd:Au sample to 2.79 Å in the 1:1 Pd:Au sample to 2.78 Å in the 3:1 Pd:Au sample. This decrease in distance has been attributed by others to the increased d−d interaction in small particles due to hybridization.[65] In addition, the Debye−Waller EXAFS terms (σ^2) for the Au−Au and Pd−Pd in the as-synthesized nanoparticle systems are all slightly higher than seen after calcination. This can be attributed to contributions from the slightly large number of surface atoms in the as-synthesized system, which would have larger σ^2 values.[80] These findings also support the HRTEM measurements in which small particle size change was observed after calcination.

In order to further test whether the rational catalyst design strategy is effective, alumina-supported 1:3 Pd:Au core−shell nanoparticles were also synthesized. Core−shell nanoparticles are interesting because they can be used as a tool for systematic investigations of the electronic properties of catalysts and can minimize the amount of precious metals, such as Pd and Pt, during the synthesis of industrial catalysts.[35,85] HRTEM images of the supported 1:3 Pd:Au core−shell catalysts indicate the presence of particles with an average particle size of 5.0 ± 1.3 nm (Figure 6A). A small particle size change from 5.0 ± 1.3 to 5.5 ± 1.9 nm is observed after calcination at 300 °C to remove the PVP stabilizer (Figure 6B). Large-area and single-particle energy-dispersive spectroscopy (EDS) analyses of the calcined core−shell nanoparticles indicated an average composition of approximately 33:67 of Pd:Au, which is in agreement with their molar percentage of respective salts during the synthesis. More importantly, the EDS line scan shown in Figure 6C strongly supports core−shell formation, with the FWHM of the two Au EDS signals (from left to right) of 6.0 and 7.0 nm, respectively, compared to 4.0 and 3.0 nm for the two Pd EDS signals. This strongly supports the fact that Pd-core−Au-shell compositional fidelity was maintained during the synthesis of the supported catalyst.

In order to further confirm that the core−shell structure was indeed fabricated in the as-synthesized xerogel-supported sample and was maintained after calcination, EXAFS characterization of the core−shell Pd−Au nanoparticles was carried out. Single-shell fits are shown in Figure 7, and the fitting results are shown in the Table 2. The formation of Pd:Au core−shell structures can be confirmed from the CNs obtained from the EXAFS fitting of the as-synthesized sample; the N_{Pd-M} CN is approximately

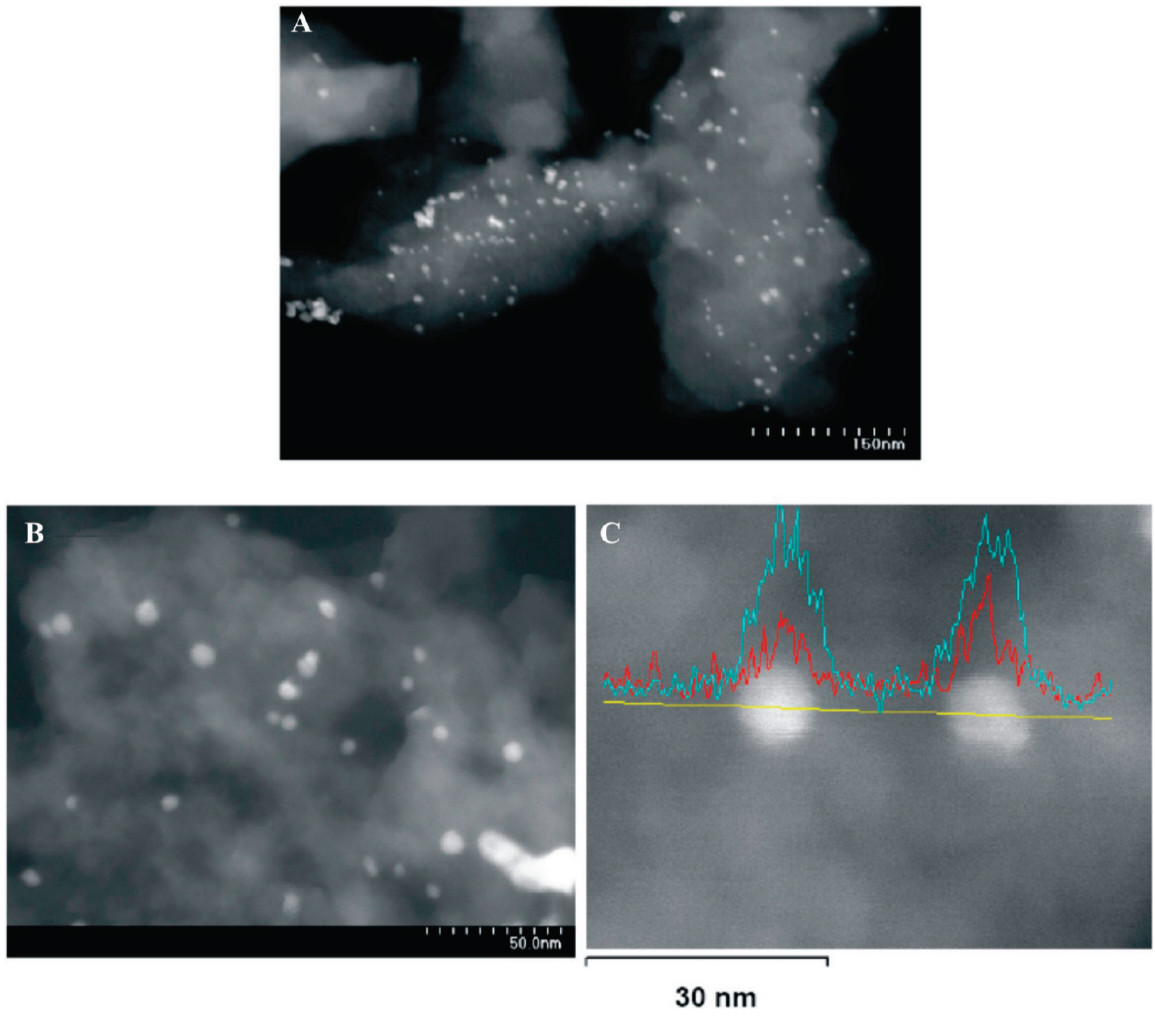

Figure 6. HRTEM images of core−shell PdAu nanoparticles (A) as-synthesized in alumina and (B) after calcination at 300 °C and (C) EDS line scan of core−shell PdAu nanoparticles in alumina after calcination at 300 °C. The blue and red EDS lines are Au and Pd, respectively.

12 and is much higher than the N_{Au-M} CN (11.0), thus confirming the presence of a Pd-rich core and Au-rich shell. In addition, the first-shell Au−Au distance is much higher than that seen for coreduced PdAu samples and is fairly similar to that seen for pure Au clusters. Unfortunately, due to instrumental availability only the Au L_{III}-edge data was collected on the calcined sample; however, the resulting N_{Au-M} coordination number of ~11.1 suggests that Au atoms are still primarily on the surface of the nanoparticle, but the higher N_{Au-Pd} suggests some alloying at the Au−Pd interface has occurred.

Finally, the XANES spectra of the Au L_{III}-edge of the series of as-synthesized coreduced PdAu nanoparticles and bulk Au foil are shown in Figure 8. The white line, the first feature after the edge jump, can be clearly seen for the Au foil and also for the pure Au nanoparticle catalysts at 11 925 eV.[56] The Au L_{III}-edge probes the transition of 2p electrons to unoccupied 5d states or empty density of states that have mainly d-character. Hence, the intensity of the white line depends on number of d-holes in the Au atoms. For bulk gold the electronic configuration would be expected to be $5d^{10}6s^{1}$; however, due to the presence of a large number of atoms, the overlap of bands becomes significant which leads to more pronounced s-p-d hybridization. Due to this s-p-d hybridization a small amount of 5d electrons is transferred to s-p states, thus resulting in an electronic configuration of $5d^{10-x}6s^{1+x}$ for bulk gold.[86,87] The weak white line in the Au-foil XANES spectra can be attributed to this depletion of the d-band. While going from the bulk to nanosized particles, the number of atoms forming the lattice decreases and hence the width of bands also decreases, which leads to less overlap of bands and, thus, less s-p-d hybridization. Consequently, the white line intensity of small Au nanoparticles should be less intense than that of the bulk, and indeed this has been documented by a number of other groups.[79,87,88]

Upon examination of the XANES data in Figure 8, it is noted that the intensity of the white line diminishes with increasing Pd content and is completely absent for 3:1 Pd:Au nanoparticles. The same trend has also been observed for the calcined samples, which confirms that no major electronic changes have occurred after calcination. Zhang et al.[79] also found that increasing Pd content in PdAu alloys has a pronounced effect in the enhanced filling of the Au d-band (an increase of the d-electron density), leading to a decrease in the white line. A possible reason for the enhanced filling of the Au d-band in the PdAu alloys is via charge transfer from the Pd s-band (and perhaps p-band) to the Au d-band.[89] A second feature in the XANES spectra in Figure 8 that merits attention is the increase in the intensity of the second band after the edge (11 935 eV) with increased Pd loading. Others have attributed changes in this second feature to distance effects in which intraatomic redistribution of charge occurs when atoms come closer together or further apart.[90] Finally, the XANES spectra of the Au L_{III}-edge for the Pd core−Au shell nanoparticles is also included in Figure 8, and a white line feature can be seen. This further supports the presence of a Pd shell−Au core structure, particularly as the white line

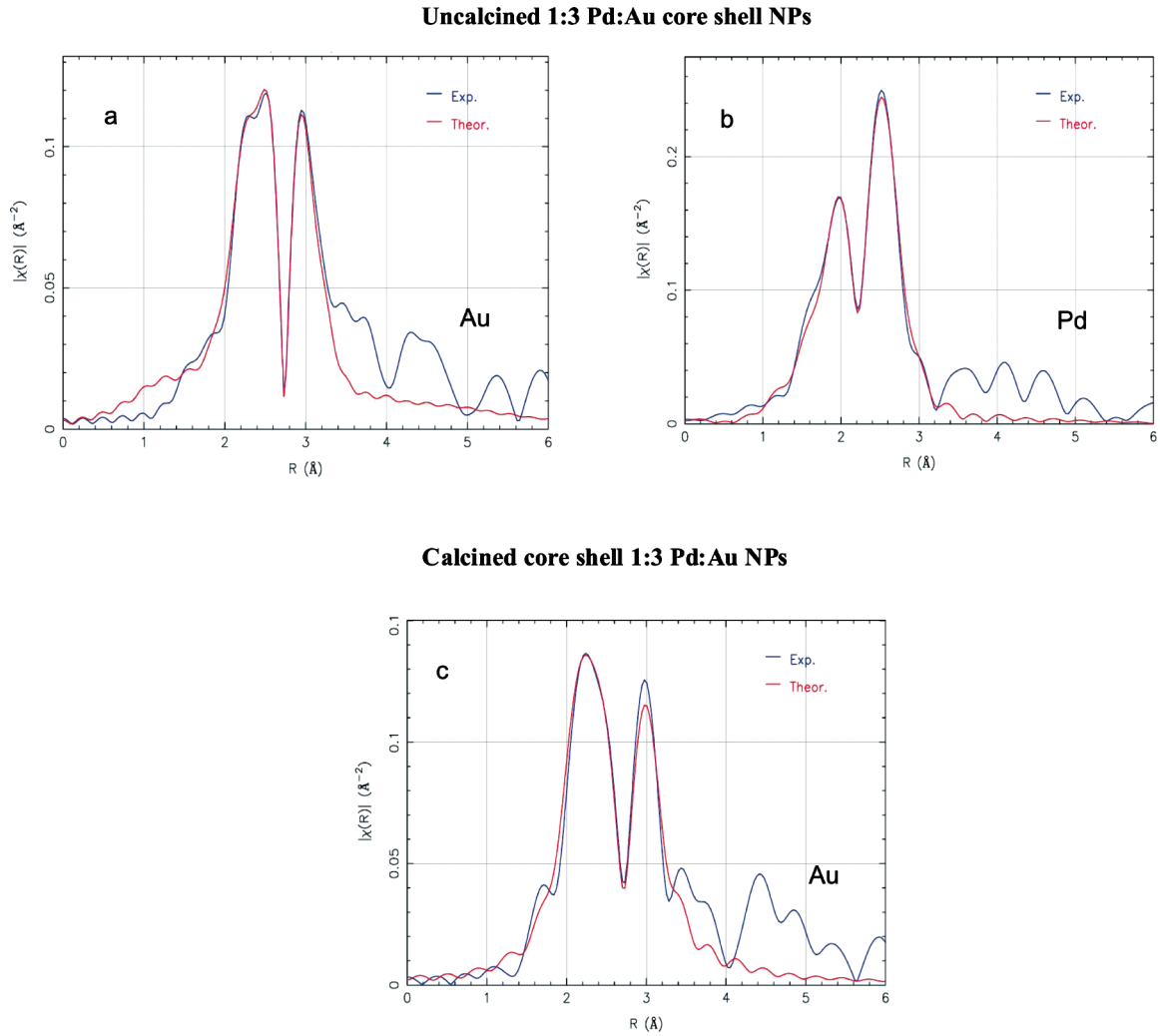

Figure 7. EXAFS fits for core−shell PdAu nanoparticles (a, b) as-synthesized in alumina and (c) after calcination at 300 °C.

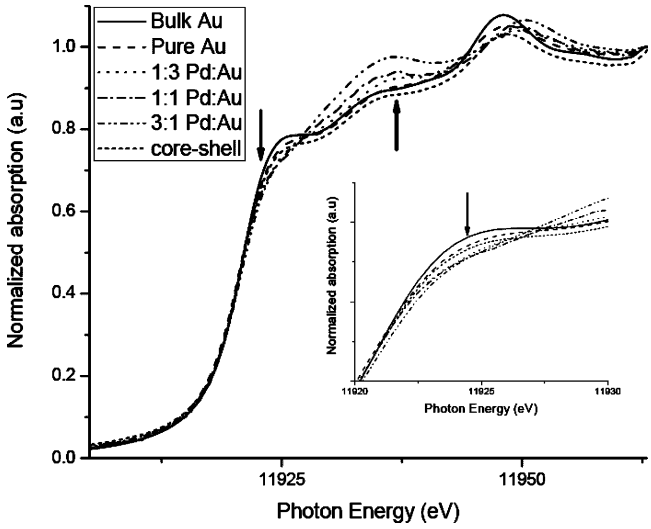

Figure 8. Au L_3-XANES spectra of as-synthesized PdAu alloy and core−shell nanoparticle series in alumina.

feature is much more intense for the 1:3 Pd:Au core−shell sample than it is for the 1:3 Pd:Au coreduced sample.

To test the catalytic activity of these catalysts, the catalytic hydrogenation of allyl alcohol was chosen as a suitable reaction. This reaction has been extensively studied on both Au and Pd metals and is therefore excellently suited to probe the catalytic activity of these nanoparticle catalysts synthesized by our methods.[24,37] The pure Pd catalyst is found to be catalytic active toward the hydrogenation of allyl alcohol with a turnover frequency (TOF) of 203 h^{-1}. For the 3:1 Pd:Au coreduced catalysts, there is a slight increase in the TOF to 210 h^{-1}. Others, including ourselves, have previously shown much higher synergetic interactions between Pd and Au;[24,25,37] the small synergetic effect here may possibly be attributed to the fact that the hydrogenation reaction was carried in water where mass-transfer limitation problems (i.e., H_2 to the catalyst surface) are a major factor.[25] The catalytic activity of calcined core−shell Pd−Au nanoparticle catalysts showed much lower catalytic activity (TOF of 60 h^{-1}) compared to that of the alloy PdAu catalysts. This lower activity can be attributed to the presence of a large number of surface Au atoms, which typically show no activity toward the hydrogenation of allyl alcohol and lend support to fairly good retention of the Pd core, Au shell structure after calcination of the nanoparticles.[24] While the catalytic results are preliminary, these results do confirm that the calcination conditions chosen produce nanoparticles that are catalytically active. More thorough high-temperature gas-phase reactions with rationally designed supported PdAu nanoparticles are currently underway in our laboratories.

4. Conclusion

The field of heterogeneous catalysis has greatly been improved by the development of nanoparticle synthesis and characterization methods. We have shown that one such improvement is the ability to rationally control nanoparticle catalyst structures during synthesis, which enables the production of catalysts with specific catalytic selectivity. A series of PVP-stabilized Au, Pd, and PdAu bimetallic nanoparticles were synthesized and then trapped in alumina matrix by sol−gel chemistry. Careful high-temperature calcinations were carried out to remove the organic PVP stabilizer and generate structurally and compositionally well-defined nanoparticles. The change in composition and internal architecture was investigated before and after calcination by TGA, HRTEM, EDS, EXAFS, and XANES. The structural investigations suggest that coreduced PdAu nanoparticles have slightly Au-rich cores and Pd-rich shells. The Au L_{III} XANES spectra reveal an increase in the d-holes of the Au 5d valence band as Au content rises in the coreduced PdAu bimetallic nanoparticle catalysts. We further showed that supported Pd core−Au shell nanoparticles can be synthesized by such methods and that the structural and geometrical integrity was maintained after the calcination step. Finally, the coreduced PdAu catalysts are found to be catalytically active toward the hydrogenation of allyl alcohol and should be active for many other catalytic reactions.

Acknowledgment. The authors acknowledge financial assistance from the National Sciences and Engineering Research Council of Canada (NSERC) and thank Ning Chen and Jeff Warner at the Canadian Light Source for assistance with XAS measurements. The XAS measurements described in this paper were performed at the Canadian Light Source, which is supported by NSERC, NRC, CIHR, and the University of Saskatchewan.

References and Notes

(1) Bond, G. C. *Chem. Rev.* **1991**, *20*, 441.
(2) Sinfelt, J. H. *Science* **1977**, *195*, 641.
(3) Sinfelt, J. H. *Acc. Chem. Res.* **1977**, *10*, 15.
(4) Sinfelt, J. H. *Acc. Chem. Res.* **1987**, *20*, 134.
(5) Toshima, N.; Yonezawa, T. *New J. Chem.* **1998**, *22*, 1179.
(6) Enache, D. I.; Edwards, J. K.; Landon, P.; Solsona-Espriu, B.; Carley, A. F.; Herzing, A. A.; Watanabe, M.; Kiely, C. J.; Knight, D. W.; Hutchings, G. J. *Science* **2006**, *311*, 362.
(7) Edwards, J. K.; Carley, A. F.; Herzing, A. A.; Kiely, C. J.; Hutchings, G. J. *Faraday Discuss.* **2008**, *138*, 225.
(8) Landon, P.; Collier, P. J.; Papworth, A. J.; Kiely, C. J.; Hutchings, G. J. *Chem. Commun.* **2002**, 2058.
(9) Solsona, B. E.; Edwards, J. K.; Landon, P.; Carley, A. F.; Herzing, A.; Kiely, C. J.; Hutchings, G. J. *Chem. Mater.* **2006**, *18*, 2689.
(10) Edwards, J. K.; Solsona, B.; Landon, P.; Carley, A. F.; Herzing, A.; Watanabe, M.; Kiely, C. J.; Hutchings, G. J. *J. Mater. Chem.* **2005**, *15*, 4595.
(11) Edwards, J. K.; Solsona, B. E.; Landon, P.; Carley, A. F.; Herzing, A.; Kiely, C. J.; Hutchings, G. J. *J. Catal.* **2005**, *236*, 69.
(12) Landon, P.; Collier, P. J.; Carley, A. F.; Chadwick, D.; Papworth, A. J.; Burrows, A.; Kiely, C. J.; Hutchings, G. J. *Phys. Chem. Chem. Phys.* **2003**, *5*, 1917.
(13) Han, Y.-F.; Zhong, Z.; Chen, F.; Chen, L.; White, T.; Tay, Q.; Yaakub, S. N.; Wang, Z. *J. Phys. Chem. C* **2007**, *111*, 8410.
(14) Ketchie, W. C.; Murayama, M.; Davis, R. J. *J. Catal.* **2007**, *250*, 264.
(15) Villa, A.; Campione, C.; Prati, L. *Catal. Lett.* **2007**, *115*, 133.
(16) Conte, M.; Carley, A. F.; Attard, G.; Herzing, A. A.; Kiely, C. J.; Hutchings, G. J. *J. Catal.* **2008**, *257*, 190.
(17) Scott, R. W. J.; Sivadinarayana, C.; Wilson, O. M.; Yan, Z.; Goodman, D. W.; Crooks, R. M. *J. Am. Chem. Soc.* **2005**, *127*, 1380.
(18) Lopez-Sanchez, J. A.; Dimitratos, N.; Miedziak, P.; Ntainjua, E.; Edwards, J. K.; Morgan, D.; Carley, A. F.; Tiruvalam, R.; Kiely, C. J.; Hutchings, G. J. *Phys. Chem. Chem. Phys.* **2008**, *10*, 1921.
(19) Herzing, A. A.; Carley, A. F.; Edwards, J. K.; Hutchings, G. J.; Kiely, C. J. *Chem. Mater.* **2008**, *20*, 1492.
(20) Pârvulescu, V. I.; Parvulescu, V.; Eudruschat, U.; Filoti, G.; Wagner, F. E.; Kübel, C.; Richards, R. *Chem. Eur. J.* **2006**, *12*, 2343.
(21) Chen, M.; Kumar, D.; Yi, C.-W.; Goodman, D. W. *Science* **2005**, *310*, 291.
(22) Wei, T.; Wang, J.; Goodman, D. W. *J. Phys. Chem. C* **2007**, *111*, 8781.
(23) Wang, D.; Villa, A.; Porta, F.; Su, D.; Prati, L. *Chem. Commun.* **2006**, 1956.
(24) Dash, P.; Dehm, N. A.; Scott, R. W. J. *J. Mol. Catal. A: Chem.* **2008**, *286*, 114.
(25) Hou, W.; Dehm, N. A.; Scott, R. W. J. *J. Catal.* **2008**, *253*, 22.
(26) Ertl, G.; Knözinger, H.; Weitkamp, J. *Handbook of Heterogeneous Catalysis*; Wiley/VCH: New York/Weinheim, 1997.
(27) Haruta, M. *Catal. Today* **1997**, *36*, 153.
(28) Hoover, N. N.; Auten, B. J.; Chandler, B. D. *J. Phys. Chem. B* **2006**, *110*, 8606.
(29) Lindner, E.; Schneller, T.; Auer, F.; Mayer, H. A. *Angew. Chem., Int. Ed.* **1999**, *38*, 2154.
(30) Schweyer, F.; Braunstein, P.; Estournes, C.; Guille, J.; Kessler, H.; Paillaud, J.-L.; Rose, J. *Chem. Commun.* **2000**, 1271.
(31) Mandal, S.; Roy, D.; Chaudhari, R. V.; Sastry, M. *Chem. Mater.* **2004**, *16*, 3714.
(32) Toshima, N.; Harada, M.; Yamazaki, Y.; Asakura, K. *J. Phys. Chem.* **1992**, *96*, 9927.
(33) Du, Y. K.; Yang, P.; Mou, Z. G.; Hua, N. P.; Jiang, L. *J. Appl. Polym. Sci.* **2006**, *99*, 23.
(34) Bönnemann, H.; Brijoux, W.; Brinkmann, R.; Dinjus, E.; Joußen, T.; Korall, B. *Angew. Chem., Int. Ed.* **1991**, *30*, 1312.
(35) Schmid, G.; Lehnert, A.; Malm, J.-O.; Bovin, J.-O. *Angew. Chem. Int. Ed* **1991**, *30*, 874.
(36) Scott, R. W. J.; Wilson, O. M.; Crooks, R. M. *Chem. Mater.* **2004**, *16*, 5682.
(37) Scott, R. W. J.; Wilson, O. M.; Crooks, R. M. *J. Phys. Chem. B* **2005**, *109*, 692.
(38) Scott, R. W. J.; Wilson, O. M.; Oh, S.-K.; Kenik, E. A.; Crooks, R. M. *J. Am. Chem. Soc.* **2004**, *126*, 15583.
(39) Lafaye, G.; Siani, A.; Marecot, P.; Amiridis, M. D.; Williams, C. T. *J. Phys. Chem. B* **2006**, *110*, 7725.
(40) Lang, H.; May, R. A.; Iversen, B. L.; Chandler, B. D. *J. Am. Chem. Soc.* **2003**, *125*, 14832.
(41) Lang, H. G.; Maldonado, S.; Stevenson, K. J.; Chandler, B. D. *J. Am. Chem. Soc.* **2004**, *126*, 12949.
(42) Zheng, N.; Stucky, G. D. *J. Am. Chem. Soc.* **2006**, *128*, 14278.
(43) Budroni, G.; Corma, A. *Angew. Chem., Int. Ed.* **2006**, *45*, 3328.
(44) Kônya, Z.; Puntes, V. F.; Kiricsi, I.; Zhu, J.; Ager, J. W.; Ko, M. K.; Frei, H.; Alivisatos, P.; Somorjai, G. A. *Chem. Mater.* **2003**, *15*, 1242.
(45) Long, C. G.; Gilbertson, J. D.; Vijayaraghavan, G.; Stevenson, K. J.; Pursell, C. J.; Chandler, B. D. *J. Am. Chem. Soc.* **2008**, *130*, 10103.
(46) Chou, J.; McFarland, E. W. *Chem. Commun.* **2004**, 1648.
(47) Song, H.; Rioux, R. M.; Hoefelmeyer, J. D.; Komor, R.; Niesz, K.; Grass, M.; Yang, P.; Somorjai, G. A. *J. Am. Chem. Soc.* **2006**, *128*, 3027.
(48) Bratlie, K. M.; Lee, H.; Komvopoulos, K.; Yang, P.; Somorjai, G. A. *Nano Lett.* **2007**, *7*, 3097.
(49) Bönnemann, H.; Endruschat, U.; Tesche, B.; Rufinska, A.; Lehmann, C. W.; Wagner, F. E.; Filoti, G.; Pârvulescu, V.; Pârvulescu, V. I. *Eur. J. Inorg. Chem.* **2000**, 819.
(50) Singh, A.; Chandler, B. D. *Langmuir* **2005**, *21*, 10776.
(51) Sun, J.; Ma, D.; Zhang, H.; Liu, X.; Han, X.; Bao, X.; Weinberg, G.; Pfänder, N.; Su, D. *J. Am. Chem. Soc.* **2006**, *128*, 15756.
(52) Min, B. K.; Wallace, W. T.; Goodman, D. W. *Surf. Sci.* **2006**, *600*, L7.
(53) Bond, G. C.; Rawle, A. F. *J. Mol. Catal. A: Chem.* **1996**, *109*, 261.
(54) Juszczyk, W.; Karpiński, Z.; Łomot, D.; Pielaszek, J.; Sobczak, J. W. *J. Catal.* **1995**, *151*, 67.
(55) Meitzner, G.; Sinfelt, J. H. *Catal. Lett.* **1995**, *30*, 1.
(56) Sinfelt, J. H.; Meitzner, G. D. *Acc. Chem. Res.* **1993**, *26*, 1.
(57) Via, G. H.; Drake, K. F.; Meitzner, G.; Lytle, F. W.; Sinfelt, J. H. *Catal. Lett.* **1990**, *5*, 25.
(58) Meitzner, G.; Via, G. H.; Lytle, F. W.; Sinfelt, J. H. *J. Phys. Chem.* **1992**, *96*, 4960.
(59) Meitzner, G.; Via, G. H.; Lytle, F. W.; Sinfelt, J. H. *Physica B* **1989**, *158*, 138.
(60) Sinfelt, J. H.; Via, G. H.; Lytle, F. W. *Catal. Rev.: Sci. Eng.* **1984**, *26*, 81.
(61) Bazin, D.; Sayers, D.; Rehr, J. J.; Mottet, C. *J. Phys. Chem. B* **1997**, *101*, 5332.
(62) Bazin, D.; Rehr, J. J. *J. Phys. Chem. B* **2003**, *107*, 12398.
(63) Hwang, B.-J.; Sarma, L. S.; Chen, J.-M.; Chen, C.-H.; Shih, S.-C.; Wang, G.-R.; Liu, D.-G.; Lee, J.-F.; Tang, M.-T. *J. Am. Chem. Soc.* **2005**, *127*, 11140.

(64) Frenkel, A. I.; Hills, C. W.; Nuzzo, R. G. *J. Phys. Chem. B* **2001**, *105*, 12689.
(65) Bus, E.; van Bokhoven, J. A. *J. Phys. Chem. C* **2007**, *111*, 9761.
(66) de Graaf, J.; van Dillen, A. J.; de Jong, K. P.; Koningsberger, D. C. *J. Catal.* **2001**, *203*, 307.
(67) Dash, P.; Scott, R. W. J. *Chem. Commun.* **2009**, 812.
(68) Jana, N. R.; Gearheart, L.; Murphy, C. J. *Chem. Mater.* **2001**, *13*, 2313.
(69) Stern, E. A.; Newville, M.; Ravel, B.; Yacoby, Y.; Haskel, D. *Physica B* **1995**, *208*, 117.
(70) Rehr, J. J.; Albers, R. C.; Zabinsky, S. I. *Phys. Rev. Lett.* **1992**, *69*, 3397.
(71) Maeland, A.; Flanagan, T. B. *Can. J. Phys.* **1964**, *42*, 2364.
(72) Ravel, B.; Newville, M. *J. Synchrotron Rad.* **2005**, *12*, 537.
(73) Wilson, O. M.; Knecht, M. R.; Garcia-Martinez, J. C.; Crooks, R. M. *J. Am. Chem. Soc.* **2006**, *128*, 4510.
(74) Creighton, J. A.; Eadon, D. G. *J. Chem. Soc., Faraday Trans.* **1991**, *87*, 3881.
(75) Zhao, M.; Crooks, R. M. *Chem. Mater.* **1999**, *11*, 3379.
(76) Hodak, J. H.; Henglein, A.; Giersig, M.; Hartland, G. V. *J. Phys. Chem. B* **2000**, *104*, 11708.
(77) Pyrz, W. D.; Buttrey, D. J. *Langmuir* **2008**, *24*, 11350.
(78) Gniewek, A.; Ziolkowski, J. J.; Trzeciak, A. M.; Zawadzki, M.; Grabowska, H.; Wrzyszcz, J. *J. Catal.* **2008**, *254*, 121.
(79) Liu, F.; Wechsler, D.; Zhang, P. *Chem. Phys. Lett.* **2008**, *461*, 254.
(80) Shibata, T.; Tostmann, H.; Bunker, B.; Henglein, A.; Meisel, D.; Cheong, S.; Boyanov, M. *J. Synchrotron Rad.* **2001**, *8*, 545.
(81) Delley, B.; Ellis, D. E.; Freeman, A. J.; Baerends, E. J.; Post, D. *Phys. Rev. B* **1983**, *27*, 2132.
(82) Chen, C.-H.; Sarma, L. S.; Chen, J.-M.; Shih, S.-C.; Wang, G.-R.; Liu, D.-G.; Tang, M.-T.; Lee, J.-F.; Hwang, B.-J. *ACS Nano* **2007**, *1*, 114.
(83) Knecht, M. R.; Weir, M. G.; Frenkel, A. I.; Crooks, R. M. *Chem. Mater.* **2008**, *20*, 1019.
(84) Remita, H.; Etcheberry, A.; Belloni, J. *J. Phys. Chem. B* **2003**, *107*, 31.
(85) Schmid, G.; West, H.; Malm, J.-O.; Bovin, J.-O.; Grenthe, C. *Chem. Eur. J.* **1996**, *2*, 1099.
(86) Wertheim, G. K. *Z. Phys. D: At., Mol. Clusters* **1989**, *12*, 319.
(87) van Bokhoven, J. A.; Miller, J. T. *J. Phys. Chem. C* **2007**, *111*, 9245.
(88) Zhang, P.; Sham, T. K. *Phys. Rev. Lett.* **2003**, 90.
(89) Marx, S.; Baiker, A. *J. Phys. Chem. C* **2009**, *113*, 6191.
(90) Pedersen, M. Ø.; Helveg, S.; Ruban, A.; Stensgaard, I.; Laegsgaard, E.; Nørskov, J. K.; Besenbacher, F. *Surf. Sci.* **1999**, *426*, 395.

JP9037182